NASA/TM—2013-217846

AIAA–2013–1075

Simulating Effects of High Angle of Attack on Turbofan Engine Performance

Yuan Liu
N&R Engineering and Management Services, Parma Heights, Ohio

Russell W. Claus, Jonathan S. Litt, and Ten-Huei Guo
Glenn Research Center, Cleveland, Ohio

February 2013

NASA STI Program . . . in Profile

Since its founding, NASA has been dedicated to the advancement of aeronautics and space science. The NASA Scientific and Technical Information (STI) program plays a key part in helping NASA maintain this important role.

The NASA STI Program operates under the auspices of the Agency Chief Information Officer. It collects, organizes, provides for archiving, and disseminates NASA's STI. The NASA STI program provides access to the NASA Aeronautics and Space Database and its public interface, the NASA Technical Reports Server, thus providing one of the largest collections of aeronautical and space science STI in the world. Results are published in both non-NASA channels and by NASA in the NASA STI Report Series, which includes the following report types:

- TECHNICAL PUBLICATION. Reports of completed research or a major significant phase of research that present the results of NASA programs and include extensive data or theoretical analysis. Includes compilations of significant scientific and technical data and information deemed to be of continuing reference value. NASA counterpart of peer-reviewed formal professional papers but has less stringent limitations on manuscript length and extent of graphic presentations.

- TECHNICAL MEMORANDUM. Scientific and technical findings that are preliminary or of specialized interest, e.g., quick release reports, working papers, and bibliographies that contain minimal annotation. Does not contain extensive analysis.

- CONTRACTOR REPORT. Scientific and technical findings by NASA-sponsored contractors and grantees.

- CONFERENCE PUBLICATION. Collected papers from scientific and technical conferences, symposia, seminars, or other meetings sponsored or cosponsored by NASA.

- SPECIAL PUBLICATION. Scientific, technical, or historical information from NASA programs, projects, and missions, often concerned with subjects having substantial public interest.

- TECHNICAL TRANSLATION. English-language translations of foreign scientific and technical material pertinent to NASA's mission.

Specialized services also include creating custom thesauri, building customized databases, organizing and publishing research results.

For more information about the NASA STI program, see the following:

- Access the NASA STI program home page at *http://www.sti.nasa.gov*

- E-mail your question to *help@sti.nasa.gov*

- Fax your question to the NASA STI Information Desk at 443–757–5803

- Phone the NASA STI Information Desk at 443–757–5802

- Write to:
  STI Information Desk
  NASA Center for AeroSpace Information
  7115 Standard Drive
  Hanover, MD 21076–1320

NASA/TM—2013-217846 AIAA–2013–1075

Simulating Effects of High Angle of Attack on Turbofan Engine Performance

Yuan Liu
N&R Engineering and Management Services, Parma Heights, Ohio

Russell W. Claus, Jonathan S. Litt, and Ten-Huei Guo
Glenn Research Center, Cleveland, Ohio

Prepared for the
51st Aerospace Sciences Meeting
sponsored by the American Institute of Aeronautics and Astronautics
Grapevine, Texas, January 7–10, 2013

National Aeronautics and
Space Administration

Glenn Research Center
Cleveland, Ohio 44135

February 2013

Acknowledgments

This work was sponsored by the Aviation Safety Program at the NASA Glenn Research Center.

Level of Review: This material has been technically reviewed by technical management.

Available from

NASA Center for Aerospace Information
7115 Standard Drive
Hanover, MD 21076–1320

National Technical Information Service
5301 Shawnee Road
Alexandria, VA 22312

Available electronically at http://www.sti.nasa.gov

Simulating Effects of High Angle of Attack on Turbofan Engine Performance

Yuan Liu
N&R Engineering and Management Services
Parma Heights, Ohio 44130

Russell W. Claus, Jonathan S. Litt, and Ten-Huei Guo
National Aeronautics and Space Administration
Glenn Research Center
Cleveland, Ohio 44135

Abstract

A method of investigating the effects of high angle of attack (AOA) flight on turbofan engine performance is presented. The methodology involves combining a suite of diverse simulation tools. Three-dimensional, steady-state computational fluid dynamics (CFD) software is used to model the change in performance of a commercial aircraft-type inlet and fan geometry due to various levels of AOA. Parallel compressor theory is then applied to assimilate the CFD data with a zero-dimensional, nonlinear, dynamic turbofan engine model. The combined model shows that high AOA operation degrades fan performance and, thus, negatively impacts compressor stability margins and engine thrust. In addition, the engine response to high AOA conditions is shown to be highly dependent upon the type of control system employed.

Nomenclature

AOA	angle of attack
CFD	computational fluid dynamics
C-MAPSS40k	Commercial Modular Aero-Propulsion System Simulation 40k
EPR	engine pressure ratio
LP	low-pressure (refers to spool)
LPC	low-pressure compressor
HARV	High Alpha Research Vehicle
HISTEC	High Stability Engine Control
HP	high-pressure (refers to spool)
HPC	high-pressure compressor
PR	operating point pressure ratio
PR_s	surge line pressure ratio
SM	stall margin
V/STOL	vertical/short takeoff and landing

1.0 Introduction

If an aircraft operates beyond the threshold of its design flight envelope, it may enter into a loss-of-control situation. Computer simulations of aircraft and their powerplants are useful tools for studying the characteristics of operation within this type of flight regime and developing recovery strategies. However, engine simulations are usually developed assuming relatively nominal flight conditions. The impact of

operating the vehicle in an unusual manner (e.g., commercial aircraft at high angle of attack) on engine performance is generally not modeled. In order to utilize computer simulations to investigate off-nominal, loss-of-control scenarios, such effects must be accounted for. This paper presents the methodology and results of simulating the effects of high angle of attack (AOA) flight on the performance of commercial aircraft turbofan engines.

High AOA flight conditions cause aerodynamic distortions in the inlet air flow entering the engine. There is an abundance of research knowledge pertaining to the relationship between AOA and inlet distortion. Not surprisingly, most investigations into inlet distortion due to high AOA operation were conducted for military-type applications. Walsh (Ref. 1) and Steenken (Ref. 2) utilized the F/A-18A High Alpha Research Vehicle (HARV) to study inlet characteristics and inlet/engine compatibility at steady-state and dynamic high-AOA conditions. It was found that high AOA flight caused high levels of radial and circumferential inlet distortion and degraded inlet pressure recovery. Compressor stalls were associated with time-varying inlet distortion during high rates of aircraft motion. Norby (Ref. 3) utilized computational fluid dynamics (CFD) simulation tools on the HARV geometry to predict steady-state and instantaneous dynamic inlet distortion patterns. Bissinger (Ref. 4) compared CFD predictions of distortion patterns and pressure recovery with experimental data for a Eurofighter inlet at high AOA.

High AOA studies involving commercial-type inlets and/or engines are more limited. Much of the research in this area was conducted within the context of tilt-nacelle vertical/short takeoff and landing (V/STOL) aircraft. Syberg (Ref. 5) performed wind tunnel testing of a high-bypass ratio turbofan engine with an inlet designed for high AOA operation. Unsteady and separated flow was observed at the operational limits of the inlet, which caused a drop in measured net thrust. Williams (Ref. 6) focused on fan blade stresses due to operating a tilt-nacelle at high AOA, but also recorded inlet distortion patterns that showed internal flow separation and ingestion of the exterior nacelle wake. Other research investigated inlet/engine coupling effects of high AOA operation, which are significant for the relatively short inlets utilized on commercial aircraft. Hodder (Ref. 7) and Larkin (Ref. 8) experimentally demonstrated that the presence of an engine delayed flow separation to higher AOA levels (versus a flow-through inlet).

The majority of both experimental and computational research studies on the effects of inlet distortion on engine performance is centered on compression system stability. Experiments with engine rigs generally utilized a distortion screen to create inlet total pressure non-uniformities. The general consensus from experimental testing on engines such as the J85-GE-13 turbojet (Ref. 9) and PW1128 low-bypass turbofan (Ref. 10) was that inlet distortion modifies the compression system performance maps, adversely shifting the surge lines. It is also known that inlet distortions are attenuated as they travel through the engine compression system (Ref. 11). Soeder (Ref. 12) showed that this attenuation occurs in a high-bypass turbofan as well.

For decades, parallel compressor theory has been the *de facto* standard for simulating the effects of inlet distortion on the engine. The technique is relatively efficient and simple to implement on either standalone compressor or full engine simulations. In its most basic form, the theory involves representing an inlet distortion as a series of different inlet boundary conditions to multiple compressor models operating in parallel (a more detailed description is provided in Section 3.0). Parallel compressor theory has been applied to the J85-GE-13 engine by researchers to predict compressor stall due to both steady-state (Refs. 13 and 14) and dynamic (Ref. 15) inlet distortions. Mazzawy (Ref. 16) and Walter (Ref. 17) used an enhanced version of parallel compressor theory on the TF30-P-3 and F100(3) low-bypass turbofan engines, respectively, to simulate distortion propagation and distortion-induced stall characteristics observed in experimental data. More recent computational efforts have utilized CFD tools to simulate the effects of inlet distortion on turbomachinery geometry. For example, Hirai (Ref. 18) investigated the effects of circumferential total pressure distortion on the flow field in a transonic compressor rotor. Yao (Ref. 19) and Gorrell (Ref. 20) simulated swirl generation and propagation caused by inlet total pressure distortion for a multistage fan.

Despite this plethora of information on the interrelationships among high AOA operation, inlet distortion, and engine performance, there is relatively limited mention in the open literature of the effects of high AOA and/or inlet distortion on overall performance parameters such as thrust. The studies on this subject have suggested that flow distortions may significantly affect engine performance through sensor measurement corruption or pressure recovery degradation (Refs. 21 and 22). It is understandable that the primary focus of inlet distortion research has been on compression system stability since rotating stall and surge are serious phenomena, especially within unconventional operational regimes such as high AOA. Nevertheless, for research into loss-of-control mitigation and recovery, the system-wide effects are also important. Therefore, this work examines, through computer simulation, the effects of high AOA operation on overall propulsion system performance.

This paper documents the methodology used to incorporate AOA/distortion effects into a turbofan engine simulation. CFD modeling tools were used to determine how different levels of AOA operation impact the performance (e.g., mass flow, pressure ratio, efficiency) of a fan/inlet representative of those used on modern commercial aircraft. For simplicity, steady-state operation was assumed for both the AOA of the inlet flow and the resulting component performance. Additionally, the CFD calculations were performed on a partial-annulus fan/inlet geometry due to computational resource limitations. Section 2.0 presents the details and results of the CFD effort. Section 3.0 describes the engine simulation used for this work: a zero-dimensional model of a generic, high-bypass, dual-spool turbofan engine capable of simulating shaft dynamics. Parallel compressor theory was applied to the engine model to assimilate the CFD data. Section 4.0 documents the results of using this combined model to simulate engine operation at various AOA levels. Additionally, the dependence of the AOA effects on the engine control system is examined. Limitations of the modeling technique and future work are discussed as well.

2.0 Computational Fluid Dynamics Simulation

2.1 Modeling Strategy

Ideally, the CFD simulation would include time-accurate flow dynamics over a three-dimensional, full-annulus geometry for a particular engine. However, this level of computing resources and information was not available at this initial stage of research. This work focuses on steady performance and utilizes a three-dimensional CFD model of an engine inlet and fan similar to those on a commercial-type transport aircraft. The model does not represent a specific commercial engine. The fan component was derived from the Energy Efficient Engine as reported in Hall (Ref. 23). The inlet was based on the geometry of a Boeing 757 nacelle. The overall strategy for the CFD simulations involved separating the problem into two flow domains: an isolated inlet with no turbomachinery (where a rapid assessment of high AOA flow could be made) and an integrated inlet/fan simulation (to assess turbomachinery performance). The two domains were analyzed with different software and meshes to employ the appropriate level of resolution for each flow region. As will be seen in the CFD results section, these calculations compare favorably with available experimental data at zero AOA.

The isolated inlet simulation consisted of unstructured mesh calculations of the 757 nacelle at different AOA flow conditions. These calculations were performed using OpenFOAM (Ref. 24). OpenFOAM has been used for a wide variety of flows and compares well with experimental data for some flow fields (Ref. 25), though it has not been validated for nacelle flow fields. The inlet model employed approximately 2 million nodes but did not include any turbomachinery geometry. Figure 1 shows an example of these calculations. These results were used to define the inlet pressure profiles for the more comprehensive inlet/fan model.

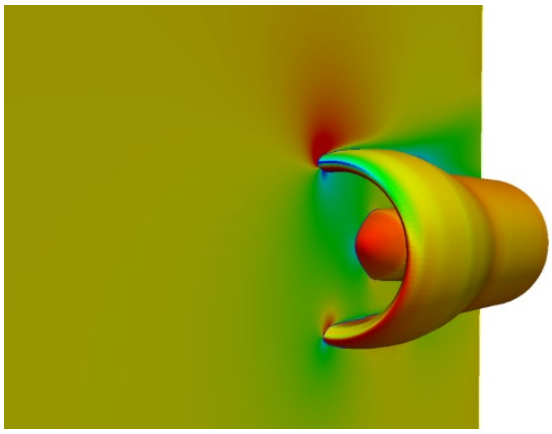

Figure 1.—Example of nacelle simulation using OpenFOAM (displaying the static pressure field for 24° AOA).

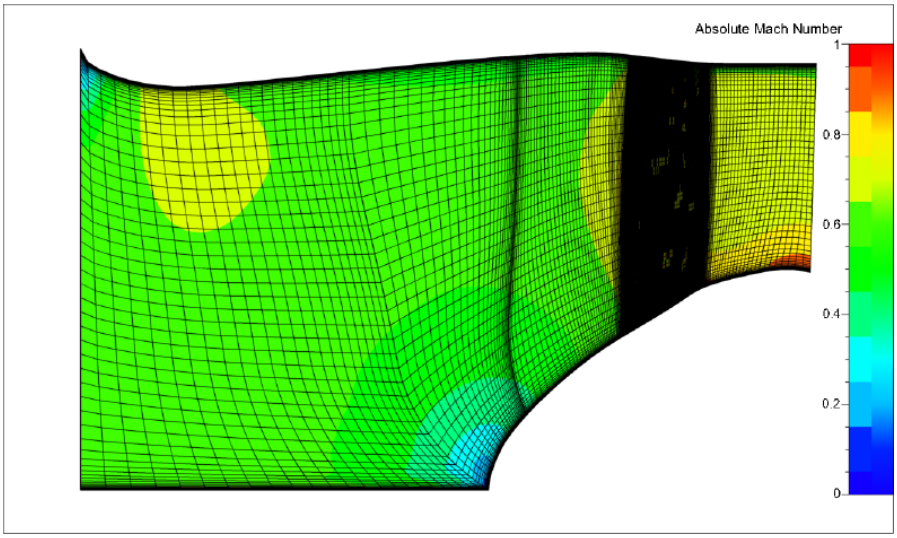

Figure 2.—Example of integrated inlet/fan simulation using FINE/Turbo (displaying circumferentially averaged absolute Mach Number with structured mesh).

Numerical simulation of the integrated inlet and fan involved solving the Reynold's Averaged Navier-Stokes equations using the Numeca FINE/Turbo code suite (Ref. 26). This software has a fully integrated suite of tools that enables rapid mesh generation, domain decomposition, flow solving, and visualization. The mesh generation can be controlled through a series of utilities that tailor the grid topology and optimization to the application-specific geometry. Typically, the defaults for the mesh generation provide good mesh characteristics; however, adjustments were made using available manual controls. The operating blade shapes (which can—in theory and practice—change as a function of centrifugal force) were provided for nominal take-off blade position. FINE/Turbo employs a variety of possible rotor/stator interface techniques, turbulence models, and differencing techniques. In this study, the steady-state options were used, including the Spalart-Almos turbulence model, the Mixing Plane approximation, and Flux Difference Splitting (second order upwind) with Min Mod limiters. Figure 2 illustrates the general flow domain of the inlet/fan simulation in FINE/Turbo. The inflow boundary is located at the entry to the inlet fairing and the domain extends beyond the fan blade. A structured mesh was used in all calculations. Figure 2 shows the fine mesh resolution around the fan blade. Figure 3 illustrates the mesh used around each blade. Each blade row was represented using 1.4 million computational nodes.

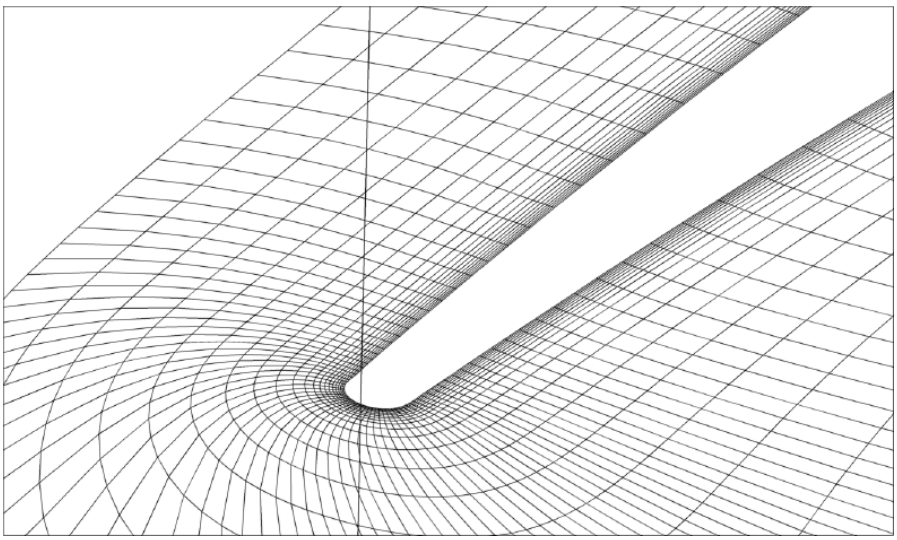

Figure 3.—Structured mesh around the fan blade used in inlet/fan simulations.

2.2 Fan Model

The combination of fan rotation and AOA variation results in an intrinsically asymmetrical problem. From the perspective of a reference frame fixed to the rotating fan blades, the incident air flow vector varies continuously as a function of circumferential location. Thus, the CFD simulation would ideally include time-accurate flow dynamics over a full-annulus (i.e., 360° extent) geometry. However, a full-annulus (32 blade passages) calculation would involve approximately 45 million nodes. Since the nature of this investigation requires simulating a large number of cases—iterating through a range of AOA values and fan operating points—a complete full-annulus simulation is considered to be too expensive in terms of time and computing resources at this stage.

A less computationally intensive approach was used for this work. To simulate the rotating turbomachinery in FINE/Turbo, the integrated inlet/fan geometry was divided into four quadrants. This simplification reduces the full-annulus simulation into four approximately 11 million-node calculations, which satisfy the memory constraints of the computational resources utilized. Each quadrant (Figure 4) consists of 8 blades. For a given AOA, each quadrant experiences a different inflow, which was specified as profiles of velocity, total pressure, and total temperature. Figure 5 provides a notional illustration of how the inflow velocity profiles differ for each quadrant. The diagrams assume a perspective situated in front of the fan looking aft. For constant non-zero AOA, the inlet/fan encounters a flow velocity with a cross flow component (Part A). However, from a rotating reference frame fixed to the blades, the cross flow is manifested as a velocity component whose direction is quadrant-dependent (Part B). Namely, quadrants 1 and 3 experience radially oriented flow; quadrants 2 and 4 experience circumferentially oriented flow. Furthermore, note that the cross flows for each radial/circumferential pair are opposite in direction. To simplify the presentation of the results, we define the cross flow directions of quadrants 1 and 2 in Part B of Figure 5 as positive AOA. Thus, to approximate the full-annulus fan performance at a given AOA, the quadrant CFD model must be run with radial and circumferential cross flows at both positive and negative AOA. The operating point of the fan was defined by the exit static pressure at the downstream boundary. AOA was specified by the ratio of cross flow velocity to axial velocity at the model inlet boundary (i.e., AOA is the inverse tangent of this ratio). The cross-plane boundary was determined using a periodic boundary condition (flow entering the domain in the circumferential direction is defined by flow exiting at the other end of the sector) that results in a further approximation of the full-annulus geometry.

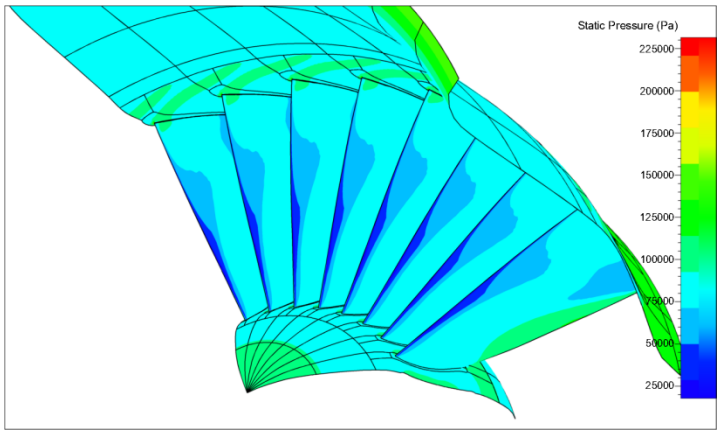

Figure 4.—Example of partial-annulus inlet/fan model in FINE/ Turbo (displaying static pressure contours calculated at zero AOA).

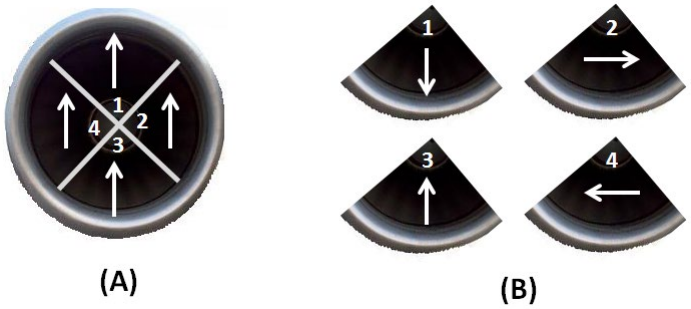

Figure 5.—Cross flow due to constant non-zero AOA (A) varies with circumferential position from a blade-fixed reference frame (B).

2.3 Results

The CFD model was used to simulate the effects of AOA variation on five different fan operating points. Figure 6 shows the locations of these points (at 0° AOA) in terms of percentage deviation of mass flow rate and pressure ratio from the design point. Each operating point is identified (see legend) by its relation in percentage to the design speed. Additionally, the label, "Low," designates the operating point as one of two on the same speed line that has the lower pressure ratio. The exit static pressure for each operating point was selected such that fan operating characteristics, such as mass flow rate, pressure ratio, and efficiency, compared favorably to experimental results at zero AOA (Ref. 27).

For each of the five operating points, the CFD model was used to simulate a range of negative and positive AOA values for both radially and circumferentially oriented cross flow. This was accomplished by varying the upstream axial-to-cross flow velocity ratio while holding exit static pressure constant. The nacelle model in OpenFOAM did not report any significant levels of total pressure or temperature variation for AOA lower than 30°. Thus, a relatively uniform pressure profile was provided to the fan model at these AOA levels. For each operating point, the fan model was used to calculate mass flow rate, pressure ratio, and efficiency for a range of AOA values. These parameters were recorded as a ratio, or "scaling factor," relative to the zero AOA case for that respective operating point. This procedure was executed for both radial and circumferential cross flow. Figure 7 depicts the variation of these scaling factors with AOA. Experimental data at non-zero AOA were not available to validate the results.

Based on the simulation results, fan performance deteriorates noticeably as the magnitude of the AOA increases despite imposing a relatively uniform total pressure profile at the inlet lip (as specified by the nacelle model). This is attributed to the increasingly off-nominal flow velocity angles the fan blades

encounter as AOA is increased. Another observation is that the performance deterioration is not symmetrical about zero AOA. Indeed, it was previously asserted that the sign of the AOA when modeling the fan quadrant simply represents the direction of the radial or circumferential cross flow seen by the blades. However, because of their rotation, the blades encounter an additional cross flow velocity component (not shown in Figure 5) that is identical for all four quadrants. Combining this cross flow due to rotation with a positive AOA cross flow produces a different resultant velocity vector than doing so with a negative AOA cross flow. Hence, the performance trends seen in Figure 7 are expected to be asymmetrical about zero AOA.

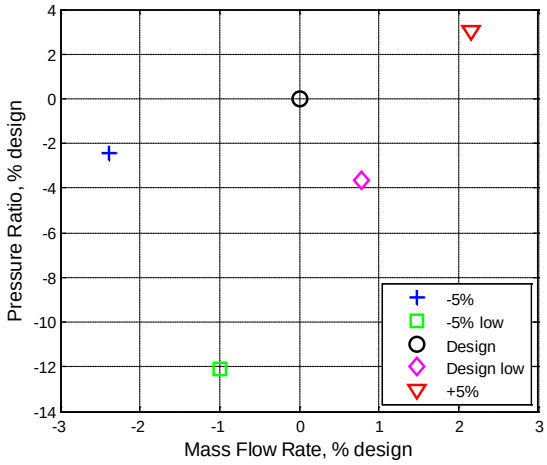

Figure 6.—CFD simulation operating points in terms of pressure ratio and mass flow rate relative to fan design point.

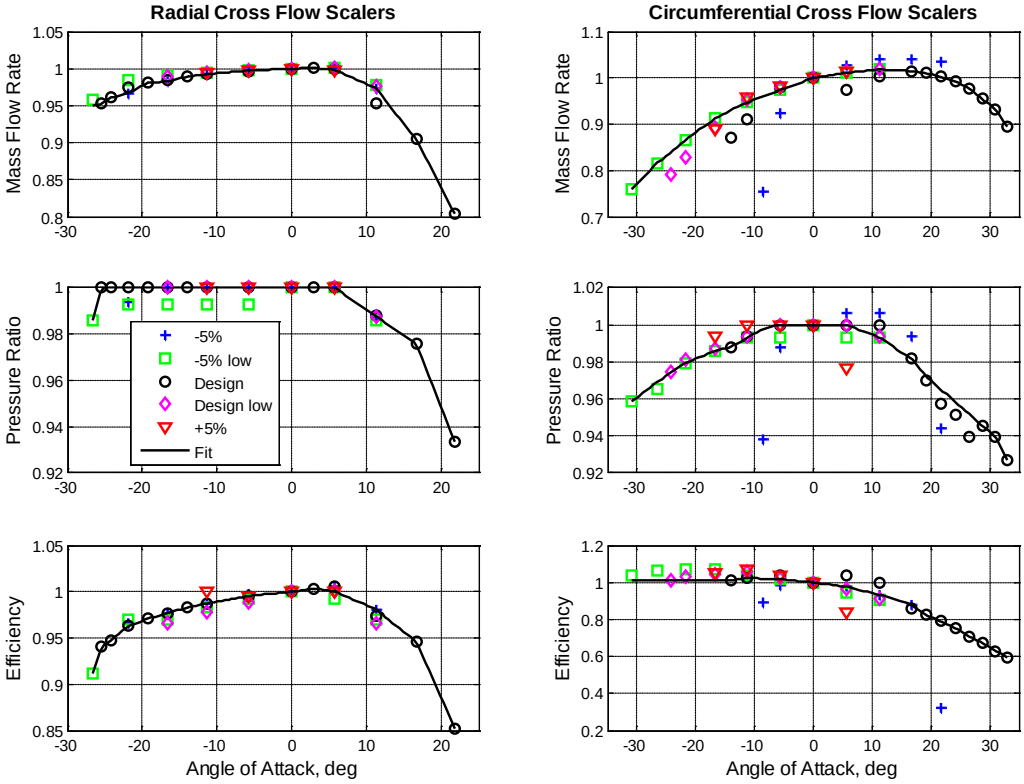

Figure 7.—CFD results for radial and circumferential cross flow sections: scaling factors for fan performance map parameters relative to zero AOA for five different operating points.

Furthermore, the relationships between AOA and the scaling factors for mass flow rate, pressure ratio, and efficiency are relatively similar for all five operating points. This statement holds more strongly with the radially oriented cross flow cases than the circumferentially oriented ones. Nevertheless, based on this observation, the scaling factors for each performance parameter are consolidated into a single trend line (denoted by the solid black lines). Conceptually, this represents the simplifying assumption that all points on the fan performance maps are scaled identically as a function of AOA, regardless of corrected speed.

The trend lines in Figure 7 show that the ability of the fan model to converge to a solution reaches a limit at approximately 30° AOA in both the positive and negative directions for most of the cases presented. However, recall that to approximate the full-annulus fan performance at a given AOA, both positive and negative AOA values for both radial and circumferential cross flow cases are required. Thus, the maximum AOA capable of being modeled by combining the quadrants is restricted by the smallest AOA magnitude encountered when the CFD fan model reaches its limit of convergence capability. As Figure 7 shows, the AOA limit for this work is approximately 21°, beyond which the fan model could not successfully converge for positive-direction, radial-oriented cross flows.

3.0 Engine Simulation

Once the effects of high AOA conditions on fan performance were established by the CFD model, parallel compressor theory was applied to a turbofan engine simulation to evaluate the impact on overall engine performance. The engine model used for this work is the Commercial Modular Aero-Propulsion System Simulation 40k (C-MAPSS40k) (Ref. 28).

3.1 Model Description

C-MAPSS40k is a zero-dimensional, nonlinear, dynamic model of a generic commercial aircraft engine implemented in the MATLAB/Simulink environment. The simulation package also contains a realistic model of the engine control system, capable of operating the engine based on fan speed or engine pressure ratio (EPR). The powerplant modeled is representative of high-bypass turbofan engines in the 40,000-pound thrust range. The rotating components of the engine are interconnected by two separate spools (Figure 8). The fan and low-pressure compressor (LPC) are powered by the low-pressure turbine through the low-speed spool; the high-pressure compressor (HPC) is powered by the high-pressure turbine via the high-speed spool. The tip and hub regions of the fan component are modeled separately. The engine bypass flow is handled solely by the fan tip model. The fan hub section is lumped with the LPC as a single compressor unit. The compressor and turbine components are modeled using performance maps (e.g., pressure ratio as function of mass flow rate and corrected speed). The two shaft rotational speeds represent the state variables of the dynamical system, allowing for simulation of transient engine operation. Volume dynamics are not accounted for in the simulation.

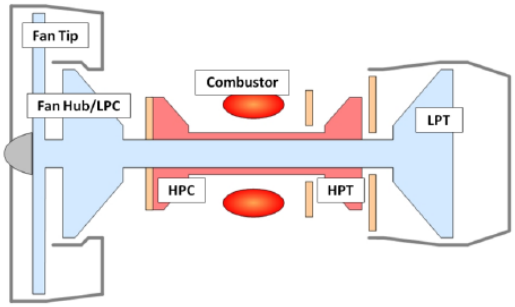

Figure 8.—Simplified diagram of C-MAPSS40k turbofan engine.

Physical inputs such as ambient parameters, fuel flow, and variable geometry parameters (e.g., stator vane and bleed valve positions) largely define the operating condition of the engine. Additionally, an independent variable must be specified to define the operating point of each rotating component. This translates into five such independent parameters for C-MAPSS40k. For the turbines, this parameter is the total pressure drop across the component. For C-MAPSS40k, the independent variable for the compression components (fan, LPC, HPC) is called "EMline." Since it is not uncommon for the characteristics on a compressor performance map to be partially vertical, specifying corrected speed and mass flow often does not uniquely determine the operating point. Thus, EMline, though not representative of any physical quantity within the engine, is used along with corrected speed to tabulate the performance map of each compression system.

To determine the values of the five independent variables, mass flow conservation constraints are enforced at five different locations throughout the engine (e.g., HPC inlet flow equals LPC exit flow less bleed flow into the bypass duct). A Jacobian matrix is calculated from the relationship between the independent variables and the constraint equations. The five independent parameters are iterated using the inverse of the matrix until the five mass flow constraints are satisfied. This procedure is executed at each simulation time step.

3.2 Parallel Compressor Theory

Parallel compressor theory is used to incorporate the CFD results into the C-MAPSS40k engine model. Parallel compressor theory is a relatively simple and well-established technique for modeling the effects of inlet distortion on compressor performance (Ref. 14). The premise involves sectioning the flow through a compressor into an arbitrary number of parallel streams. The flow path split is area-based and should approximate the inlet distortion pattern to be modeled. For instance, Figure 9 illustrates modeling a distortion in inlet total pressure and/or temperature of 60° circumferential extent. Thus, the flow is split into two streams: one through a 60° section and the other through a 300° section. Typically, the performance map of the original compressor model is applied to each flow path after being scaled down in terms of mass flow by the relative size of the section. For example, as shown in Figure 9, the abscissa (mass flow rate) of the compressor map is scaled proportionally to the size of each parallel section; the ordinate (pressure ratio), however, remains unscaled for both sections.

To resolve the parallel compressor streams, the flow paths are assumed to exit into the same static pressure. Overall mass flow is the sum of the mass flow through the individual sections. Overall exit total pressure is an area-weighted average across all sections. Overall exit total temperature is a mass flow-weighted average. Note that if the inlet conditions are identical for each flow path, the parallel compressor model recovers the performance of the original compressor model regardless of how the parallel sections are defined.

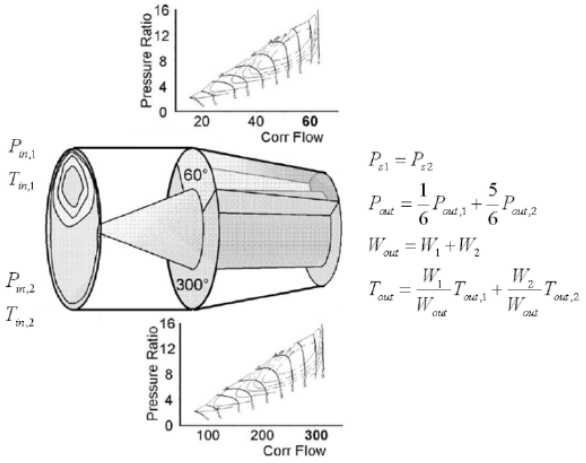

Figure 9.—Illustration of the principles of parallel compressor theory.

3.3 Implementation

For this work, the parallel compressor technique is applied to the fan tip and the fan hub/LPC components of the C-MAPSS40k engine simulation. Since the CFD model simulates the fan in quadrants, each of these two components is split into four equally sized sections. This introduces six new compressor components (three additional fan tip models, three additional fan hub/LPC models) into the engine simulation. Thus, the Jacobian matrix is expanded and recalculated to include six additional independent variables (i.e., EMlines). These new variables are accounted for by imposing the aforementioned uniform exit static pressure distribution for the fan tip and the fan hub/LPC components. Hence, the iterative engine balance procedure remains well-defined (11 independent variables, 5 flow constraints, 6 static pressure constraints).

The conventional approach for simulating inlet distortion using parallel compressor theory is to vary the inlet condition of each parallel compressor model to approximate the distortion pattern under study. For this work, however, the inlet conditions of all eight compressor models are identically defined. Recall that the nacelle CFD model did not reveal variations in total pressure or temperature for AOA levels less than 30°. However, the fan model showed deterioration in performance due to changes in the velocity field encountered by the blades caused by non-zero AOA. Therefore, to model AOA effects, the performance maps for each of the parallel compressor components are modified by scaling them according to the CFD results. For example, to simulate an AOA of 15°, the results shown in Figure 7 are used to obtain four sets of scaling factors corresponding to ±15° radial and ±15° circumferential cross flows. Each set contains scaling factors for mass flow rate, pressure ratio, and efficiency. The scaling factors are then appropriately applied to each of the four parallel compressor components for both the fan tip and the fan hub/LPC models.

4.0 Results and Discussion

Engine performance is inextricably linked to the control system. Thus, three simulation test cases are presented and analyzed in this section:

1) Open Loop: fuel flow held constant
2) Fan Speed Control: fuel flow calculated from feedback control of fan speed
3) EPR Control: fuel flow calculated from feedback control of engine pressure ratio

The environmental conditions are: altitude of 1000 ft; Mach 0.2; standard altitude-based ambient temperature. The test cases differ in the type of control strategy employed. The primary aim of an engine control system is to govern the thrust produced by the engine by modulating fuel flow. Since thrust is an unmeasurable quantity during flight, the control system generally controls on a variable that is closely correlated to thrust. For the control system modeled in C-MAPSS40k, this variable can be either fan speed or engine pressure ratio (EPR: the ratio of low-pressure turbine exit pressure to fan inlet pressure). “Open loop” operation, where no control algorithm is utilized and fuel flow is directly specified, acts as a baseline of comparison for the other two cases. The engine is operated at the full-power throttle setting (power lever angle of 80°) for the duration of each test case. Thus, at zero AOA, thrust produced by the engine is identical for all cases regardless of control mode.

To assess its effects on engine performance, AOA is linearly increased from 0° to 21° over 60 sec (Figure 10) for each of the three test cases. Recall that 21° is the maximum AOA capable of being simulated by combining the fan quadrant results due to CFD convergence limitations. Loss-of-control flight scenarios are generally dynamic in nature; changes in AOA may be not only large but also abrupt. Therefore, it is important to note that the CFD results for fan operation at different AOA are steady-state due to time and resource constraints. Namely, they do not capture any flow dynamics that may occur even while holding AOA constant. Moreover, as AOA is increased, fan performance is modified by interpolating through the scaling factors provided by the CFD data (Figure 7). Consequently, any features that are unique to dynamically changing AOA are not modeled. Instead, it is more appropriate to interpret the AOA transient shown in Figure 10 as a slow, quasi-steady progression towards higher levels of AOA. The significance of this limitation is recognized and future efforts are planned to address it.

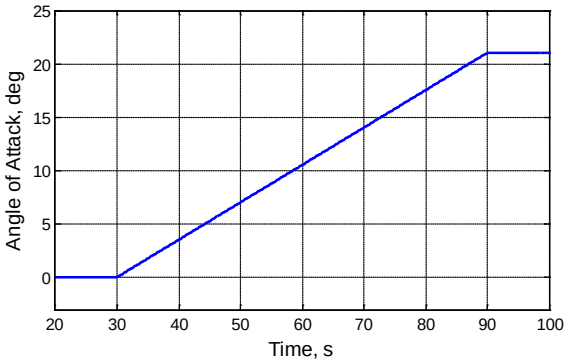

Figure 10.—Quasi-steady AOA progression from 0° to 21° applied to engine model.

4.1 Fan and Compressor Stall Margins

Figure 11 compares the pressure rise characteristics (i.e., pressure ratio versus corrected mass flow rate) at 0° and 21° AOA for each of the four parallel fan hub/LPC models. The numbering corresponds to the diagrams in Figure 5. The characteristics at zero AOA (black lines) are identical for all four compressor models. However, at 21° AOA, scaling factors from the CFD analysis were applied to the characteristics (blue lines), varying them from model to model. The red line is the surge line as defined by the C-MAPSS40k engine model. In order to simulate the effects of high AOA on the fan and LPC stability characteristics, the surge line is assumed to be static. This assumption is consistent with parallel compressor theory. As expected, inlet distortion negatively impacts compressor stability. Figure 11 shows that the speed lines of three of the four parallel compressors (1, 3, and 4) shift left towards the surge line, effectively decreasing the surge-free operational envelope of the fan hub/LPC. The fan tip performance maps are not shown but exhibit similar patterns with increasing AOA levels since the same scaling factors are applied.

The proximity of the operating point of a compressor component to the surge line is quantified by stall margin. The stall margin (*SM*) of an operating point is conventionally defined as:

$$SM = \left(\frac{PR_S}{PR} - 1\right) 100\% \tag{1}$$

In this equation, *PR* is the operating pressure ratio and PR_s is the surge line pressure ratio at the operating mass flow rate. According to parallel compressor theory, the overall compressor is assumed to become unstable (i.e., surge or rotating stall) when at least one of the parallel compressor sections is unstable. Hence, for this work, the overall compressor stall margin is calculated as the minimum of the stall margins of the four parallel compressor models.

Figure 12 shows the stall margin time histories for the fan tip, fan hub/LPC, and HPC as AOA is increased from 0° to 21°. The results suggest that the type of fuel control utilized does not significantly impact the stall margin characteristics. Not surprisingly, increasing AOA causes significant drops in fan and LPC stall margins. As previously noted, the fan and LPC performance maps are directly impacted by the simulated inlet distortion effects, decreasing their surge-free range of operation. However, the effect of AOA variation on HPC stall margin is relatively small. As stated in the literature review, it has been shown that flow non-uniformities due to inlet distortion are usually attenuated as they pass through a compression system. In a turbofan engine configuration, the HPC is shielded by the LPC and fan and thus encounters less severe flow distortion. Additionally, the HPC model was not split into parallel components for this study. Therefore, any change in HPC stall margin is entirely due to movement of the operating point (as opposed to modifications to the performance map).

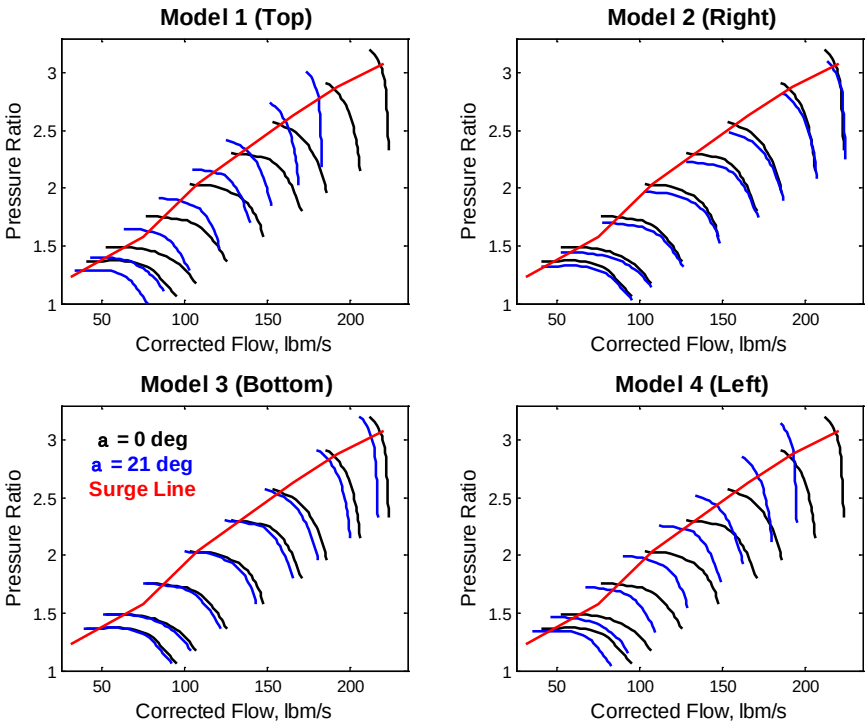

Figure 11.—Scaling of performance maps for the fan hub/LPC parallel compressor models.

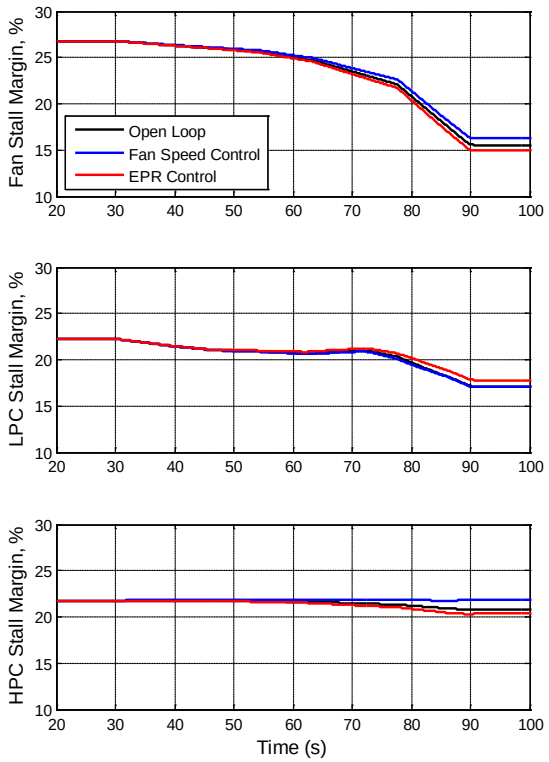

Figure 12.—Response of fan/LPC/HPC stall margins to increasing AOA.

4.2 Engine Control Parameters

Figure 13 shows the fuel flow rate supplied to the engine as AOA is increased. As previously mentioned, fuel flow is held at a constant value for the open loop case. The fuel flow levels for all three cases are identical when AOA is zero (up to the 30-sec mark) since the engine is operated at the same full-power setting throughout the experiments. However, as AOA is increased, the fan speed and EPR control algorithms react differently when computing the fuel flow rate.

When evaluating the effects of AOA variation on engine response, it is important to note that performance degradation of the fan or LPC (e.g., decrease in pressure ratio and/or mass flow) generally reduces the amount of power required to maintain its rotational speed. This relationship applies to all three cases regardless of the control scheme used. However, the effects can be most clearly observed in the open-loop case where fuel flow rate is fixed. Figure 14 shows the response of fan speed, core speed, and EPR during the AOA transient. As AOA is increased, the power required by the fan and LPC to maintain their rotational speeds decreases due to performance deterioration. Furthermore, the power required by the HPC also decreases due to the reduced mass flow rate. However, because the performance capability of the turbines is unaffected, the unchanged fuel flow rate creates a positive power imbalance on both the low-pressure (LP) and high-pressure (HP) spools. Consequently, fan and core speeds increase during open-loop operation.

Similar analysis can be applied to the fan speed and EPR control schemes. Since fan performance deteriorates with increasing AOA, less power is required to maintain constant fan speed. Hence, the fan speed control system commands a lower fuel flow rate. With respect to EPR, it is important to note that inlet distortion decreases the pressure rise capabilities of the fan and LPC. This effect results in a reduction in EPR for the open loop and fan speed control cases, even though it was found that pressure ratio across the HPC (not shown) remains relatively constant for both cases. To maintain a constant EPR level, higher pressure ratios across the fan and LPC are required. Thus, as AOA increases, the EPR control system increases fuel flow to accelerate the engine to higher speeds.

4.3 Engine Thrust

Figure 15 shows the effects of AOA on total net thrust and its constituents (bypass thrust and core thrust). As the nomenclature suggests, bypass thrust refers to the thrust generated by acceleration of the air through the bypass duct. Likewise, core thrust is generated by acceleration of the gas through the engine core. According to Figure 15, a reduction in total thrust accompanies the increase in AOA. However, the type of fuel control method employed has a noticeable impact on the magnitude of the thrust loss. Using the thrust level at zero AOA as the baseline for comparison, total thrust decreases by 7.5 percent if fuel flow is held constant (open loop). Thrust loss is approximately 3.4 percent for EPR control and 13 percent for fan speed control.

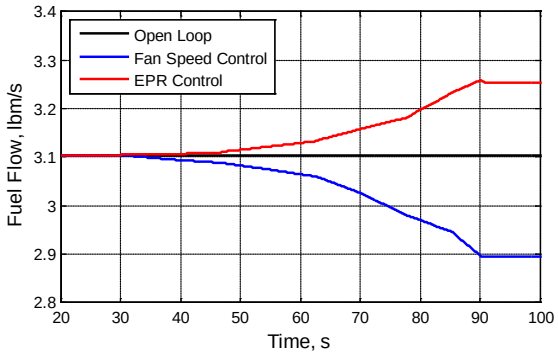

Figure 13.—Fuel flow rate command for different fuel control scheme cases.

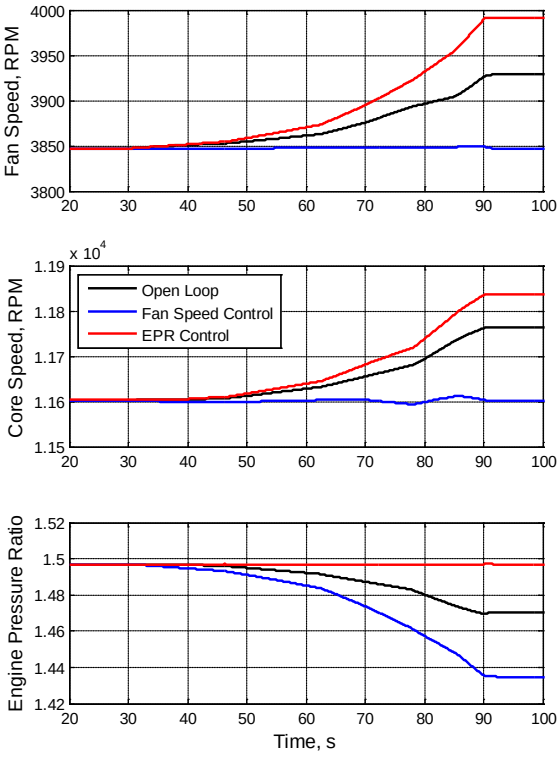

Figure 14.—Response of fan speed, core speed, and engine pressure ratio to increasing AOA.

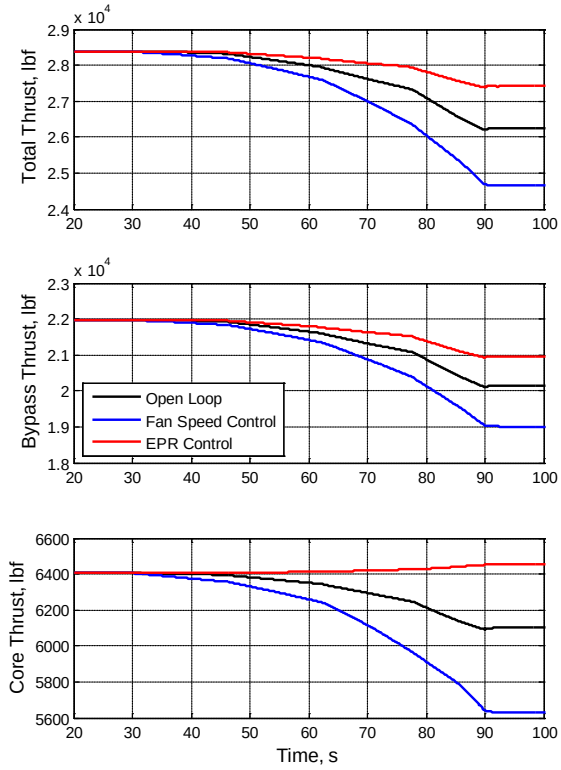

Figure 15.—Response of total thrust, thrust due to bypass flow, and thrust due to core flow to increasing AOA.

An examination of the bypass and core thrust components elucidates the cause for these differences. When fan performance is degraded by high AOA effects, loss in bypass thrust is inevitable for all control schemes. Moreover, for high-bypass turbofan engines, the bypass mass flow accounts for the majority of the total engine thrust produced. Thus, all three cases exhibit overall thrust loss as well. However, the engine operating under EPR control exhibits the least amount of bypass thrust loss. As explained previously, the EPR control system reacts to high AOA by increasing fuel flow. The resulting LP spool acceleration partially mitigates the bypass thrust loss due to fan performance deterioration. Additionally, the HP spool acceleration is sufficient to maintain a nearly constant core thrust despite the AOA variation. Similarly, maintaining constant fuel flow also increases both spool speeds but not to the levels required to maintain constant EPR. Hence, the open loop case exhibits more losses in both bypass and core thrust than the EPR control case. Finally, by maintaining constant fan speed, the engine is unable to compensate for fan performance losses. In fact, the HP spool decelerates as well due to the decrease in fuel flow. Therefore, the engine operating under fan speed control is most detrimentally affected by the high AOA conditions.

4.4 Discussion

The simulation results show that the inlet distortion induced by high AOA levels have an overall negative impact on engine performance. Selection of control mode does not seem to significantly impact stall margins, though this assertion should be investigated in more detail with higher fidelity compressor stability models. These models may need to include effects of volume dynamics within the engine. Moreover, with enhanced computational resources, the CFD efforts should be expanded to include the effects of AOA on the fan surge line.

However, the results also demonstrate that evaluation of AOA effects cannot be done with an isolated model of the engine. Namely, the magnitude of the deterioration in engine performance is sensitive to the type of control system utilized. The results suggest that fuel control based on fan speed causes the engine to react poorly to high AOA since the fan, which is responsible for the majority of the total engine thrust, is subjected to the brunt of the adverse performance effects. On the other hand, an EPR-based control system essentially compensates for the fan performance degradation to a certain extent by increasing spool speeds. However, it is recognized that the simulations conducted did not assume any total pressure variations within the inlet. Indeed, the EPR control system would be more sensitive to AOA if there were an accompanied change in inlet pressure, and particularly if such a pressure defect were to corrupt inlet sensor measurements.

An additional observation revealed by the simulation results is that there is a change in the robustness of the engine response to inlet distortion as the AOA level varies. For instance, as shown in Figure 12, the fan and LPC stall margins decrease more sharply after the 75-sec mark, which corresponds to an AOA of approximately 16°. Likewise, the rate of loss in engine thrust (Figure 15) is more severe at AOA values greater than 16°. In fact, for the case of EPR control, total thrust loss is approximately 1 percent at 16° AOA, as opposed to 3 percent by the end of the transient at 21° AOA. These characteristics are logical when viewed within the context of civil aviation. The inlet and fan of a turbofan engine intended for such aircraft would be designed to operate efficiently at relatively low AOA levels. Thus, the engine model and CFD data capture to a certain extent this desired nonlinearity in the response of engine performance to AOA variation.

5.0 Conclusions

The effects of high angle of attack (AOA) operation on the performance of a high-bypass turbofan engine were investigated using a suite of simulation tools: three-dimensional computational fluid dynamics (CFD) software, parallel compressor theory, and a zero-dimensional dynamic turbofan engine model. This paper described the methodology used to combine these resources. The simulation studies found that the deterioration of fan performance due to high AOA causes the engine to experience an

overall thrust loss. Furthermore, the severity of the thrust loss is sensitive to the type of engine control strategy utilized. Analysis of the simulation results concluded that with all other factors identical (e.g., no corruption of inlet pressure measurements), a turbofan engine controlled based on engine pressure ratio exhibits noticeably less thrust loss than one using fan speed.

The results and analysis presented in this paper are preliminary since several simplifying assumptions were made—the most significant of which is the application of CFD to a partial-annulus inlet and fan geometry. Indeed, such "parallelization" is prominent in inlet distortion studies using the parallel compressor theory. However, the focus of this overall research is the impact on the engine by, not (just) inlet distortion patterns, but high AOA flows. Analysis of this inherently asymmetrical problem will benefit from a full-annulus inlet and fan CFD simulation, which is the topic of immediate future work. Continuing efforts will also address other important limitations, such as the steady-state nature of the results presented in this paper. Application of the simulation to aircraft loss-of-control investigations necessitates accounting for the complex flow dynamics inherent to these types of flight scenarios.

References

1. Walsh, K.R., Yuhas, A.J., Williams, J.G., and Steenken, W.G., "Inlet Distortion for an F/A-18A Aircraft During Steady Aerodynamic Conditions up to 60° Angle of Attack," NASA Technical Memorandum, TM-104329, April 1997.
2. Steenken, W.G., Williams, J.G., Yuhas, A.J., and Walsh, K.R., "An Inlet Distortion Assessment During Aircraft Departures at High Angle of Attack for an F/A-18A Aircraft," NASA Technical Memorandum, TM-104328, March 1997.
3. Norby, W.P., Ladd, J.A., and Yuhas, A.J., "Dynamic Inlet Distortion Prediction with a Combined Computational Fluid Dynamics and Distortion Synthesis Approach," NASA Contractor Report, CR-198053, September 1996.
4. Bissinger, N.C. and Jost, M., "Thrust Vectoring for Advanced Fighter Aircraft – High Angle of Attack Intake Investigations," Defense Technical Information Center, 2001.
5. Syberg, J., "Low Speed Test of a High-Bypass-Ratio Propulsion System with an Asymmetric Inlet Designed for a Tilt-Nacelle V/STOL Airplane," NASA Contractor Report, CR-152072, January 1978.
6. Williams, R.C., Diedrich, J.H., and Shaw, R.J., "Turbofan Blade Stresses Induced by the Flow Distortion of a VTOL Inlet at High Angles of Attack," NASA Technical Memorandum, TM-82963, January 1983.
7. Hodder, B.K., "An Investigation of Engine Influence on Inlet Performance," NASA Contractor Report, CR-166136, 1981.
8. Larkin, M.J and Schweiger, P.S., "Ultra High Bypass Nacelle Aerodynamics; Inlet Flow-Through High Angle of Attack Distortion Test," NASA Contractor Report, CR-189149, July 1992.
9. Braithwaite, W.M, Graber, Jr., E.J., and Mehalic, C.M., "The Effects of Inlet Temperature and Pressure Distortion on Turbojet Performance," AIAA/SAE 9th Propulsion Joint Specialists Conference, Las Vegas, Nevada, 5-7 November 1973.
10. Mehalic, C.M., "Effect of Spatial Inlet Temperature and Pressure Distortion on Turbofan Engine Stability," 24th AIAA/ASME/SAE/ASEE Joint Propulsion Conference, Boston, Massachusetts, 11-13 July 1988.
11. de Bogdan, C.E., Dicus, J.H., Evans, D.G., and Soeder, R.H., "Effect of a 180°-Extent Inlet Pressure Distortion on the Internal Flow Conditions of a TF30-P-3 Engine," NASA Technical Memorandum, TM X-3267, September 1975.
12. Soeder, R.H. and Bobula, G.A., "Effect of Steady-State Pressure Distortion on Inlet Flow to a High-Bypass-Ratio Turbofan Engine," NASA Technical Memorandum, TM-82964, October 1982.
13. Daniele, C.J. and Teren, F., "Prediction of Compressor Stall for Distorted and Undistorted Flow By Use of a Multistage Compressor Simulation on the Digital Computer," AIAA 13th Aerospace Sciences Meeting, Pasadena, California, 20-22 January 1975.

14. Milner, E.J., “Analytical Prediction of the Performance and Stability of a J85-13 Compressor with Distorted Inlet Flow,” NASA Technical Memorandum, TM X-3515, May 1977.
15. Wenzel, L.M. and Blaha, R.J., “Analysis of Dynamic Inlet Distortion Applied to a Parallel Compressor Model,” NASA Technical Memorandum, TM X-3522, May 1977.
16. Mazzawy, R.S. and Banks, G.A., “Modeling and Analysis of the TF30-P-3 Compressor System with Inlet Pressure Distortion,” NASA Contractor Report, CR-134996, April 1976.
17. Walter, W.A. and Shaw, M., “Distortion Analysis for F100(3) Engine,” NASA Contractor Report, CR-159754, January 1980.
18. Hirai, K., Kodama, H., Nozaki, O., Kikuchi, K., Tamura, A., and Matsuo, Y., “Unsteady Three-Dimensional Analysis of Inlet Distortion in Turbomachinery,” AIAA-1997-2735, July 1997.
19. Yao, J., Gorrell, S.E., and Wadia, A.R., “A Time-Accurate CFD Analysis of Inlet Distortion Induced Swirl in Multistage Fans,” 43rd AIAA/ASME/SAE/ASEE Joint Propulsion Conference and Exhibit, Cincinnati, Ohio, 8-11 July 2007.
20. Gorrell, S.E., Yao, J., and Wadia, A.R., “High Fidelity URANS Analysis of Swirl Generation and Fan Response to Inlet Distortion,” 44th AIAA/ASME/SAE/ASEE Joint Propulsion Conference and Exhibit, Hartford, Connecticut, 21-23 July 2008.
21. Kurzke, J., “Effects of Inlet Flow Distortion on the Performance of Aircraft Gas Turbines,” Journal of Engineering for Gas Turbines and Power, Vol. 130, July 2008.
22. “Inlet Total-Pressure-Distortion Considerations for Gas-Turbine Engines,” SAE AIR1419 Rev. A, 1999.
23. Hall, E. and Owen, P., “Energy Efficient Engine HP/LP Spool Analysis,” NASA Contractor Report, CR-2008-785, 2008.
24. OpenFOAM, Software Package, Ver. 2.0.1, OpenCFD Ltd. (ESI Group), Bracknell, United Kingdom, 2010.
25. “Foam CFD,” URL: http://www.foamcfd.org [cited 11 December 2012].
26. Vilmin, S., Lorrain, E., Hirsch, C.H., and Swoboda, M., “Unsteady Flow Modeling Across the Rotor/Stator Interface Using the Nonlinear Harmonic Method,” ASME Turbo Expo 2006: Power for Land, Sea, and Air (GT2006), Barcelona, Spain, 8-11 May 2006.
27. Cline, S.J., Kutney, J.T., Halter, P.H., and Sullivan, T.J., “Energy Efficient Engine: Fan and Quarter-Stage Component Performance Report,” NASA Contractor Report, CR-168070, January 1983.
28. May, R.D., Csank, J., Lavelle, T.M., Litt, J.S., and Guo, T., “A High-Fidelity Simulation of a Generic Commercial Aircraft Engine and Controller,” 46th AIAA/ASME/SAE/ASEE Joint Propulsion Conference and Exhibit, Nashville, Tennessee, 25-28 July 2010.

REPORT DOCUMENTATION PAGE	Form Approved OMB No. 0704-0188

1. REPORT DATE *(DD-MM-YYYY)*	2. REPORT TYPE	3. DATES COVERED *(From - To)*
01-02-2013	Technical Memorandum	

4. TITLE AND SUBTITLE
Simulating Effects of High Angle of Attack on Turbofan Engine Performance

5a. CONTRACT NUMBER

5b. GRANT NUMBER

5c. PROGRAM ELEMENT NUMBER

6. AUTHOR(S)
Liu, Yuan; Claus, Russell, W.; Litt, Jonathan, S.; Guo, Ten-Huei

5d. PROJECT NUMBER

5e. TASK NUMBER

5f. WORK UNIT NUMBER
WBS 284848.02.05.03.02.03

7. PERFORMING ORGANIZATION NAME(S) AND ADDRESS(ES)
National Aeronautics and Space Administration
John H. Glenn Research Center at Lewis Field
Cleveland, Ohio 44135-3191

8. PERFORMING ORGANIZATION REPORT NUMBER
E-18622

9. SPONSORING/MONITORING AGENCY NAME(S) AND ADDRESS(ES)
National Aeronautics and Space Administration
Washington, DC 20546-0001

10. SPONSORING/MONITOR'S ACRONYM(S)
NASA

11. SPONSORING/MONITORING REPORT NUMBER
NASA/TM-2013-217846

12. DISTRIBUTION/AVAILABILITY STATEMENT
Unclassified-Unlimited
Subject Category: 07
Available electronically at http://www.sti.nasa.gov
This publication is available from the NASA Center for AeroSpace Information, 443-757-5802

13. SUPPLEMENTARY NOTES

14. ABSTRACT
A method of investigating the effects of high angle of attack (AOA) flight on turbofan engine performance is presented. The methodology involves combining a suite of diverse simulation tools. Three-dimensional, steady-state computational fluid dynamics (CFD) software is used to model the change in performance of a commercial aircraft-type inlet and fan geometry due to various levels of AOA. Parallel compressor theory is then applied to assimilate the CFD data with a zero-dimensional, nonlinear, dynamic turbofan engine model. The combined model shows that high AOA operation degrades fan performance and, thus, negatively impacts compressor stability margins and engine thrust. In addition, the engine response to high AOA conditions is shown to be highly dependent upon the type of control system employed.

15. SUBJECT TERMS
Aircraft engine performance; Aircraft engine simulation

16. SECURITY CLASSIFICATION OF:			17. LIMITATION OF ABSTRACT	18. NUMBER OF PAGES	19a. NAME OF RESPONSIBLE PERSON
a. REPORT	b. ABSTRACT	c. THIS PAGE			STI Help Desk (email:help@sti.nasa.gov)
U	U	U	UU	24	19b. TELEPHONE NUMBER *(include area code)* 443-757-5802